

# Charge, spin, and orbital degrees of freedom in manganites: Mean-field slave-boson approach

P. Schlottmann

*Department of Physics, Florida State University, Tallahassee, Florida 32306, USA*

(Received 14 October 2005; revised manuscript received 6 March 2006; published 15 June 2006)

The phase diagram of  $\text{La}_{1-x}\text{Ca}_x\text{MnO}_3$  is studied using a mean-field slave-boson formulation for  $e_g$  electrons in two orbitals and classical  $t_{2g}$  spins  $S$  oriented in the magnetic configurations of the  $A$ ,  $B$ ,  $C$ , and  $G$  phases as a function of  $x$ . The manganese ions are in a mixed valent state of two magnetic configurations  $\text{Mn}^{4+}$  and  $\text{Mn}^{3+}$ , with all  $3d$  electrons coupled ferromagnetically via Hund's rule. The multiple occupancy of the  $e_g$  levels is excluded at each site by a large Coulomb energy. The  $e_g$  electrons hop between Mn sites with amplitude  $t$  giving rise to the ferromagnetic double exchange, which competes with the antiferromagnetic superexchange  $J$  between the  $t_{2g}$  spins of the ions. The  $e_g$  electrons couple to the lattice degrees of freedom via the Jahn-Teller effect. The model has only two parameters, namely,  $J/t$  and the Jahn-Teller energy. We obtain that only the  $A$  and  $C$  phases can exhibit a Jahn-Teller distortion.

DOI: [10.1103/PhysRevB.73.214428](https://doi.org/10.1103/PhysRevB.73.214428)

PACS number(s): 75.30.Et, 71.27.+a, 71.28.+d, 75.10.Lp

## I. INTRODUCTION

The rich phase diagram of  $\text{La}_{1-x}\text{Ca}_x\text{MnO}_3$  (LCMO) (Refs. 1–8) is the consequence of the interplay of charge, spin, orbital, and lattice degrees of freedom. The end compounds  $\text{LaMnO}_3$  and  $\text{CaMnO}_3$  are antiferromagnetic insulators, while for intermediate  $x$  the system is either a ferromagnetic metal or a charge-ordered antiferromagnet and may display phase separation.<sup>9</sup> The Jahn-Teller coupling to the lattice<sup>10–12</sup> manifests itself in changes of the Mn-O-Mn bond lengths and angles,<sup>13</sup> as well as orbital order.<sup>14</sup> There are several other manganite systems<sup>8</sup> but LCMO appears to be the only alloy forming over the entire concentration range,  $0 \leq x \leq 1$ .

The Mn ions form a nearly simple cubic lattice with one oxygen ion located approximately on the center of each side and the trivalent La or divalent Ca atoms at the body center of the cube. The  $\text{O}^{2-}$  ions mediate the binding between the Mn ions, while the role of La and Ca doping is to provide conduction electrons.<sup>15</sup> The Mn ions are in a mixed trivalent ( $3d^4$ ) and tetravalent ( $3d^3$ ) state. In cubic or nearly cubic symmetry the five  $3d$  levels are split into a  $t_{2g}$  triplet and an  $e_g$  doublet. With octahedral coordination the  $t_{2g}$  states have lower energy than the  $e_g$  orbitals, so that the three  $t_{2g}$  orbitals are all singly occupied with their spins coupled to form a total spin  $S=3/2$ . The  $e_g$  orbitals, on the other hand, are empty for  $\text{Mn}^{4+}$  and occupied by one  $3d$  electron in  $\text{Mn}^{3+}$ , ferromagnetically correlated with the  $t_{2g}$  electrons due to Hund's rule to form a total spin  $S^* = 2$ . The intermediate valence character of the Mn ions arises then from the hopping of the  $e_g$  electrons.

In a previous publication<sup>16</sup> we studied a cubic lattice of mixed-valent Mn ions with the  $t_{2g}$  spins (treated classically) oriented in the spin arrangements of the  $A$ ,  $B$ ,  $C$ , and  $G$  phases of the manganites.<sup>2</sup> The multiple occupancy of the  $e_g$  levels at each site is prevented by a large Coulomb interaction, which is taken into account with auxiliary bosons in the mean-field approximation. The  $e_g$  electrons are allowed to hop between nearest neighbor sites with amplitude  $t$ , which gives rise to the ferromagnetic double exchange.<sup>17,18</sup> We obtained the band structure for the  $e_g$  electrons and the ground-state energy for each of the phases. For a given doping  $x$  the

phase diagram then only depends on one parameter, namely,  $J/t$ . Our calculation yields the correct sequence of phases as a function of  $x$  for  $J/t$  of the order of a few percent.

The Mn-O-Mn bond-length depends on the relative spin orientation of the two  $t_{2g}$  spins. Experimentally ferromagnetic bonds are found to be larger than antiferromagnetic bonds. We introduced this dependence on the bond-length as a second, fine-tuning, parameter.<sup>16</sup> Adjusting the hopping matrix element  $t$  and the superexchange integral  $J$  accordingly, we obtain an improved agreement with the rich phase diagram of  $\text{La}_{1-x}\text{Ca}_x\text{MnO}_3$ .

In this paper we extend our calculation to include the Jahn-Teller coupling to the lattice. A Jahn-Teller distortion lifts the degeneracy of the  $e_g$  levels and changes the band structure. This leads to corrections to the ground state energies of the different phases and hence to a modified phase diagram. Only the  $A$  and  $C$  phases have a significant energy gain due to lattice distortions and the region of stability of these phases grows at the expense of the  $B$  and  $G$  phases.

The rest of this paper is organized as follows. In Sec. II the model for electronic, spin, and Jahn-Teller interactions is introduced, as well as the corresponding mean-field slave-boson version for the different phases. The mean-field equations are then solved numerically and the energy is minimized. In Sec. III the different phases and the phase diagram with Jahn-Teller distortion are discussed. Conclusions follow in Sec. IV.

## II. MODEL

The Hamiltonian is written as  $H=H_t+H_m+H_{JT}$ , where  $H_t$  represents the hopping of the  $e_g$  electrons between the Mn sites on a simple cubic lattice,  $H_m$  is the magnetic energy arising from the superexchange between the  $t_{2g}$  spins, and  $H_{JT}$  is the Jahn-Teller coupling to the lattice.

### A. Electronic and magnetic interactions

The nearest neighbor hopping Hamiltonian for the  $e_g$  electrons is given by<sup>16,19</sup>

$$\begin{aligned}
H_t = & -\mu \sum_{jM^*m} |jS^*M^*m\rangle \langle jS^*M^*m| \\
& -t \sum_{\langle jl \rangle m_j m_l \sigma M_j M_l M_j^* M_l^*} (SM_{j, \frac{1}{2}} \sigma | S_{\frac{1}{2}} S^* M_j^* ) \\
& \times (SM_{l, \frac{1}{2}} \sigma | S_{\frac{1}{2}} S^* M_l^* ) \{ |jSM_j\rangle \langle jS^*M_j^*m_j| \\
& \times \hat{M}_{m_j m_l}(\mathbf{R}_{jl}) |lS^*M_l^*m_l\rangle \langle lSM_l| + \text{H.c.} \}. \quad (1)
\end{aligned}$$

Here the bra and ket denote the states of the  $\text{Mn}^{4+}$  configuration represented by a spin  $S(=3/2)$  and  $z$  projection  $M$ , and the states of the  $\text{Mn}^{3+}$  configuration of spin  $S^*=S+\frac{1}{2}$  and spin projection  $M^*$ . The localized  $3d$  electrons are then all ferromagnetically correlated (first Hund's rule). The Clebsch-Gordan coefficients select the spin components and are needed to preserve the spin rotational invariance.  $j$  labels the sites on a simple cubic lattice. The index  $m=x^2-y^2$ ,  $z^2$  labels the  $e_g$  orbitals and  $\sigma$  is the spin component of the  $e_g$  electron. The  $\text{Mn}^{3+}$  states have in addition a label  $m$  to indicate which of the  $e_g$  states is occupied. The completeness condition for the states requires that at every site

$$\sum_{M^*m} |jS^*M^*m\rangle \langle jS^*M^*m| + \sum_M |jSM\rangle \langle jSM| = 1, \quad (2)$$

which excludes the multiple occupancy of the  $e_g$  levels, i.e., they can only be empty or occupied by one electron. This corresponds to an implicit infinite on-site Coulomb repulsion.

The first term in Eq. (1) determines the Fermi energy or chemical potential  $\mu$  for the itinerant electrons, while the second term corresponds to the nearest neighbor intersite hopping. The sum is over all the nearest neighbor pairs  $\langle jl \rangle$  and  $\mathbf{R}_{jl}$  is the vector joining the sites  $j$  and  $l$ . The hopping matrix  $\hat{M}_{m_j m_l}(\mathbf{R}_{jl})$  depends on  $\mathbf{R}_{jl}$ , i.e.,  $\hat{M}_x=(2\hat{I}+\hat{\tau}_z+\sqrt{3}\hat{\tau}_x)/4$ ,  $\hat{M}_y=(2\hat{I}+\hat{\tau}_z-\sqrt{3}\hat{\tau}_x)/4$ , and  $\hat{M}_z=(\hat{I}-\hat{\tau}_z)/2$ . Here  $\hat{I}$  and  $\hat{\tau}_i$  are the identity and Pauli matrices for the orbital pseudospin of components  $(x^2-y^2, z^2)$ . These hopping matrices are determined by the overlap of the asymptotes of the  $e_g$  wave functions. The fact that  $x^2-y^2$  and  $z^2$  orbitals on neighboring sites have in general nonzero overlap implies that  $m$  is not a good quantum number.

The magnetic energy  $H_m$  arises from the superexchange of the  $t_{2g}$  spins mediated by the oxygen atoms and depends on the spin configuration of each phase. As in Ref. 16 we consider the spin arrangements of the phases A, B, C, and G of  $\text{La}_{1-x}\text{Ca}_x\text{MnO}_3$ .<sup>2</sup> In the mean field the Heisenberg superexchange reduces to  $H_m=-\alpha JS^2N$ , where  $\alpha_A=-1$ ,  $\alpha_B=-3$ ,  $\alpha_C=+1$ , and  $\alpha_G=+3$ . Here  $N$  is the number of Mn sites. The coupling strength  $J$  can be estimated from the transition temperature of the end compounds and should be of the order of 100 times smaller than the hopping  $t$ .

### B. Jahn-Teller coupling

$H_{\text{JT}}$  consists of two terms, namely, the elastic deformation energy of the lattice and the coupling of the  $e_g$  electrons to the phonons. This coupling then locally lifts the degeneracy of the  $e_g$  levels by distorting the lattice. Three normal modes

of vibration of the  $\text{MnO}_6$  octahedra have to be considered, which correspond to the irreducible representations  $\Gamma_{1g}(A_{1g})$  and  $\Gamma_{3g}(E_g)$ .<sup>20</sup> The former is the breathing mode  $Q_1$  of the  $\text{MnO}_6$  octahedron, in which the symmetry is not reduced but the volume is changed. This mode requires a large elastic energy and does not lift the degeneracy of the  $e_g$  levels, so that we keep  $Q_1=0$ . More important are the  $\Gamma_{3g}$  modes, which have been defined and parametrized by Kanamori<sup>20</sup>

$$Q_2 = (X_1 - X_4 - Y_2 + Y_5)/\sqrt{2},$$

$$Q_3 = (2Z_3 - 2Z_6 - X_1 + X_4 - Y_2 + Y_5)/\sqrt{6}, \quad (3)$$

where  $X_1-X_4$  is the elongation of the octahedron in the  $x$  direction, etc., and  $Q_1=(X_1-X_4+Y_2-Y_5+Z_3-Z_6)/\sqrt{3}$ . The Jahn-Teller Hamiltonian for site  $j$  is

$$H_{\text{JT}}^j = (C_{\text{JT}}/2)(Q_{j2}^2 + Q_{j3}^2) + 2g(Q_{j2}\hat{\tau}_{jx} + Q_{j3}\hat{\tau}_{jz}), \quad (4)$$

where  $C_{\text{JT}}$  is proportional to the elastic constant  $c_{11}-c_{12}$ ,  $g$  is the coupling constant, and  $\hat{\tau}_x$  and  $\hat{\tau}_z$  are Pauli matrices acting on the two  $e_g$  orbitals. We parametrize  $Q_{j2}=(g/C_{\text{JT}})q_j\sin(\xi_j)$  and  $Q_{j3}=(g/C_{\text{JT}})q_j\cos(\xi_j)$  and obtain

$$\begin{aligned}
H_{\text{JT}} = & \frac{E_{\text{JT}}}{2} \sum_j q_j^2 + 2E_{\text{JT}} \sum_{jM_j^*m_j'} q_j |jS^*M_j^*m_j'\rangle \\
& \times [\hat{\tau}_x \sin(\xi_j) + \hat{\tau}_z \cos(\xi_j)]_{m_j' m_j} \langle jS^*M_j^*m_j|, \quad (5)
\end{aligned}$$

where  $E_{\text{JT}}=g^2/C_{\text{JT}}$ . As  $\xi_j$  varies from 0 to  $2\pi$  all possible volume-conserving distortions of the octahedron are generated. Equation (5) is to be minimized with respect to  $q_j$  and  $\xi_j$ .

### C. Slave-boson mean-field approximation

Following Ref. 16 we introduce slave-boson creation and annihilation operators<sup>21</sup>  $b_{jM}^\dagger$  and  $b_{jM}$ , which act as projectors onto the states of the  $\text{Mn}^{4+}$  configuration with spin component  $M$  at site  $j$ , and fermion operators for the  $\text{Mn}^{3+}$  states at the site  $j$ ,  $d_{jM^*m}^\dagger$ , and  $d_{jM^*m}$ . The completeness relation equivalent to the condition (2) is now

$$\sum_M b_{jM}^\dagger b_{jM} + \sum_{M^*m} d_{jM^*m}^\dagger d_{jM^*m} = 1. \quad (6)$$

Transitions between configurations are described by the operators  $|jSM\rangle \langle jS^*M^*m| = b_{jM}^\dagger d_{jM^*m}$ . The total Hamiltonian in the auxiliary space is now given by

$$\begin{aligned}
H = & -\alpha JS^2N + \frac{E_{\text{JT}}}{2} \sum_j q_j^2 + \sum_{jM_j^*m_j'} d_{jM_j^*m_j'}^\dagger \\
& \times \{ 2E_{\text{JT}}q_j[\hat{\tau}_x \sin(\xi_j) + \hat{\tau}_z \cos(\xi_j)] - \mu \hat{I} \}_{m_j' m_j} d_{jM_j^*m_j} \\
& -t \sum_{\langle jl \rangle m_j m_l \sigma M_j M_l M_j^* M_l^*} (SM_{j, \frac{1}{2}} \sigma | S_{\frac{1}{2}} S^* M_j^* ) \\
& \times (SM_{l, \frac{1}{2}} \sigma | S_{\frac{1}{2}} S^* M_l^* ) \{ d_{jM_j^*m_j}^\dagger b_{jM_j} \\
& \times \hat{M}_{m_j m_l}(\mathbf{R}_{jl}) b_{lM_l}^\dagger d_{lM_l^*m_l} + \text{H.c.} \}, \quad (7)
\end{aligned}$$

subject to the constraint (6), which restricts the model to the physical subspace. The above slave-boson formulation is exact, i.e., it does not contain approximations with respect to the original Hamiltonian.

The spin-projections  $M_j = \pm S$  of the  $t_{2g}$  moments are then determined by the magnetic phase. The spin projection of the  $\text{Mn}^{3+}$  ion is  $M_j^* = \pm S + \sigma$  and hence the spin component  $\sigma$  of the  $e_g$  electron is a good quantum number.  $\sigma$  is either parallel or antiparallel to  $M_j$  yielding a Clebsch-Gordan coefficient equal to 1 or  $1/\sqrt{2S+1}$ , respectively. We denote these coefficients  $a_{j\sigma}$  and the index  $M_j^*$  of the fermion operators can be replaced by  $\sigma$ , i.e.,  $d_{j\sigma m}$ .

Following Ref. 16 we study Hamiltonian (7) subject to the constraint (6) in the mean-field approximation. We assume a uniform occupancy of all the sites, hence eliminating the possibility of phase separation,<sup>9</sup> an effect that has been observed in several experiments. In the mean-field (saddle-point) approximation<sup>22</sup> boson operators are replaced by their expectation values. Since all Mn sites have the same valence we have  $\langle b_{jM_j} \rangle = \langle b_{jM_j}^\dagger \rangle = b$  for  $M_j = S$  or  $M_j = -S$ , depending on the magnetic configuration, and all others are zero. The constraint (6) is incorporated via Lagrange multipliers  $\lambda_j$ . In this case  $\lambda_j = \lambda$  and  $q_j = q$  are independent of the site. The mean-field Hamiltonian is now

$$\begin{aligned}
H_{\text{MF}} = & -\alpha JS^2 N + NE_{\text{JT}} q^2 / 2 - N\lambda(1 - b^2) \\
& + \sum_{j\sigma m'_j m_j} d_{j\sigma m'_j}^\dagger \{ 2E_{\text{JT}} q [ \hat{\tau}_x \sin(\xi_j) + \hat{\tau}_z \cos(\xi_j) ] \\
& + (\lambda - \mu) \hat{I}_{m'_j m_j} d_{j\sigma m_j} - tb^2 \sum_{\langle j'l \rangle \sigma m_j m_l} a_{j\sigma} a_{l\sigma} \\
& \times [ d_{j\sigma m_j}^\dagger \hat{M}_{m_j m_l}(\mathbf{R}_{jl}) d_{l\sigma m_l} + \text{H.c.} ] \}. \quad (8)
\end{aligned}$$

All four phases have different magnetic unit cells. While the unit cell of the  $B$  phase has only one ion, the ones of the  $A$ ,  $C$ , and  $G$  phases have two Mn ions.<sup>2</sup> The Brillouin zones of the  $A$ ,  $C$ , and  $G$  phases are then contained in the simple cubic one of the  $B$  phase. To facilitate a direct comparison between the phases we adopt the simple cubic Brillouin zone for all phases. The redundant information contained for the  $A$ ,  $C$ , and  $G$  phases is then taken care of by a factor 1/2 whenever we sum over the  $\mathbf{k}$  states.

The band structure for the  $e_g$  electrons is obtained by Fourier transforming and diagonalizing Eq. (8). For each phase there are four bands arising from the two  $e_g$  levels and the two sites per unit cell. In the case of the  $B$  phase they arise from the two  $e_g$  levels and the spin. Without Jahn-Teller coupling these dispersions are discussed in Ref. 16. We denote the diagonal states with a tilde, i.e.,  $\tilde{d}_{\mathbf{k}\sigma\alpha}^\dagger$ , where  $\alpha = 1, \dots, 4$ , and the corresponding energies with  $E'_\alpha(\mathbf{k})$ . The occupation numbers  $\langle \tilde{d}_{\mathbf{k}\sigma\alpha}^\dagger \tilde{d}_{\mathbf{k}\sigma\alpha} \rangle$  are given by Fermi functions. The ground state energy is then

$$\begin{aligned}
E_{\text{GS}} = & -\alpha JS^2 N + NE_{\text{JT}} q^2 / 2 - N\lambda(1 - b^2) \\
& + \sum_{\mathbf{k}\alpha} [ \lambda - \mu + E'_\alpha(\mathbf{k}) ] f [ \lambda - \mu + E'_\alpha(\mathbf{k}) ], \quad (9)
\end{aligned}$$

which is minimized with respect to  $b$  and  $\lambda$ . This yields two

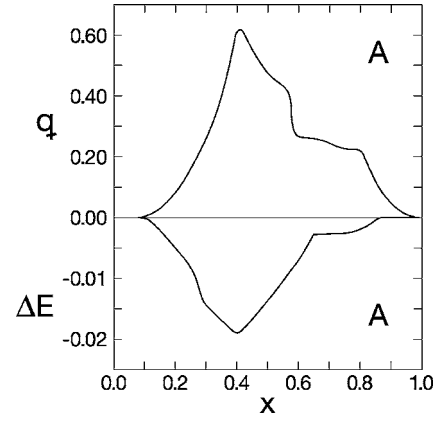


FIG. 1. Amplitude  $q$  of the Jahn-Teller distortion and energy gain  $\Delta E$  due to the Jahn-Teller coupling as a function of  $x$  for the  $A$  phase for  $E_{\text{JT}} = 0.1t$ . The parameter  $\xi$  equals  $\pi$  for all  $x$ .

transcendental equations, which are solved self-consistently. In addition the energy has to be minimized with respect to  $q$  and  $\xi$ . For most situations we assumed that  $\xi$  is the same at each site. Note that in Eq. (9) the sum over  $\sigma$  (phases  $A$ ,  $C$ , and  $G$ ) cancels the factor 1/2 that arises for using the cubic Brillouin zone instead of the reduced one.

### III. RESULTS

In this section we study the Jahn-Teller distortion induced cooperatively by the anisotropy of the  $e_g$ -electron dynamics. For the numerical study we considered  $E_{\text{JT}} = 0.1t$ . The Jahn-Teller distortions monotonically grow with  $E_{\text{JT}}$ , but there is no qualitative change of properties unless  $E_{\text{JT}}$  is very large. In the latter limit only one orbital effectively contributes.

#### A. A phase

In the  $A$  phase of  $\text{La}_{1-x}\text{Ca}_x\text{MnO}_3$  the spins are ferromagnetically oriented in  $x$ - $y$  planes and these planes are antiferromagnetically correlated along the  $z$  direction. The magnetic unit cell consists of two sites having opposite  $t_{2g}$ -spin orientation. Both spin projections of the  $e_g$  electron give rise to the same band dispersion.

Due to the layered magnetic structure, the hopping is anisotropic. This gives rise to a lattice distortion. The equilibrium value of  $q$  and the energy reduction  $\Delta E$  per Mn site caused by the distortion is displayed in Fig. 1. The number of  $e_g$  electrons is  $N(1-x)$ , so that for  $x \rightarrow 1$ , both  $q$  and  $\Delta E$  have to vanish. In the limit  $x \rightarrow 0$  the constraint (6) inhibits the  $e_g$  electrons from hopping and consequently the effect of the electron dynamics is again small. This situation is discussed in more detail below. A large distortion is only to be expected for intermediate  $x$ . The irregular dependence of both,  $q$  and  $\Delta E$ , with  $x$  arises from the band structure. As discussed above and in Ref. 16 there are four bands and numerous van Hove singularities. The energy and  $q$  are determined by integrating over the occupied states.

The lowest energy corresponds to  $\xi = \pi$  for all  $x$ . This is seen in Fig. 2 which shows the energy ( $H_t + H_{\text{JT}}$ ) as a function of  $\xi$  for  $x = 0.4$  and  $0.8$ . The effect is much larger and the

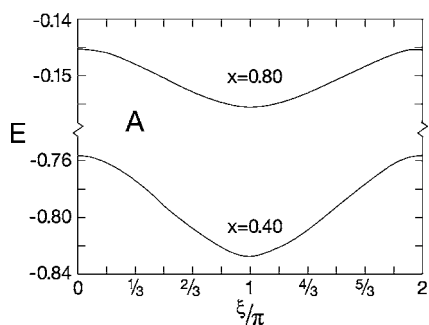


FIG. 2. Energy  $E$  corresponding to  $H_I + H_{JT}$  as a function of  $\xi$  for  $x=0.40$  and  $x=0.80$  in the  $A$  phase for  $C_{JT}=0.1t$ . The minimum of the energy is at  $\xi=\pi$ .

minimum is more pronounced for  $x=0.4$ .  $\xi=\pi$  corresponds to distortions of the octahedron such that  $X_1 - X_4 = Y_2 - Y_5 = qg/C_{JT}\sqrt{6}$  and  $Z_3 - Z_6 = -2qg/C_{JT}\sqrt{6}$ , i.e., while expanding in the  $x$ - $y$  plane it contracts in the  $z$  direction by keeping its volume constant. We have also allowed different  $\xi$  values for the two sublattices, but the energy minimum corresponds to equal  $\xi$  for all sites. For the  $A$  phase, if a larger value of  $q$  is chosen (an out-of-equilibrium value) it is possible to move the minimum as a function of  $\xi$  away from  $\pi$ .

The above explains the contraction of the  $c$  axis. The  $A$  phase has in addition staggered long-range orbital order with alternating components of the orbitals  $3x^2 - r^2$  and  $3y^2 - r^2$ . Such antiferro-orbital order requires a unit cell with four Mn ions, two in each adjacent ferromagnetically ordered  $x$ - $y$  planes. The two orbital sublattices arise if  $\xi = \pi \pm \xi_o$ , where if  $\xi_o$  is small the amplitude of the staggered long-range order is small and if  $\xi_o = \pi/3$  the orbitals are fully ordered. The order is only stabilized with an intersite interaction. Each O ion is shared by two adjacent  $MnO_6$  octahedra. If the common O ion moves toward a Mn site it compresses that octahedron but stretches the other one. The restoring force induces the intersite coupling.

### B. $B$ phase

In the  $B$  phase all the  $t_{2g}$  spins are ferromagnetically correlated and the unit cell contains only one Mn ion. The bands for  $e_g$  electrons with spin parallel to  $t_{2g}$  spins are much more dispersive than the minority spin electrons. The spin configuration does not inhibit the hopping in any direction (the Clebsch-Gordan coefficients are all the same for a given spin-component) and the dispersion for each spin-component is cubic. A Jahn-Teller distortion is then not expected for this phase. Indeed the minimum of energy is found for  $q=0$ . The ground state energy is then the same as in Ref. 16.

Fixing  $q$  at a finite value and varying  $\xi$  from 0 to  $2\pi$  yields no change in the energy (within error bars). This calculation was carried out for  $x=0.2, 0.5$ , and  $0.8$ . Hence, there is no preferred direction for  $\xi$  and all linear combinations of  $e_g$  orbitals have the same energy. This isotropy is a separate test for the absence of a Jahn-Teller distortion.

Remarkable is that in the range  $0.4 \leq x \leq 0.65$  the energy curve  $E(q)$  is not only isotropic in  $\xi$  but also rather flat for small  $q$ . In other words, the quadratic dependence in  $q$  of the

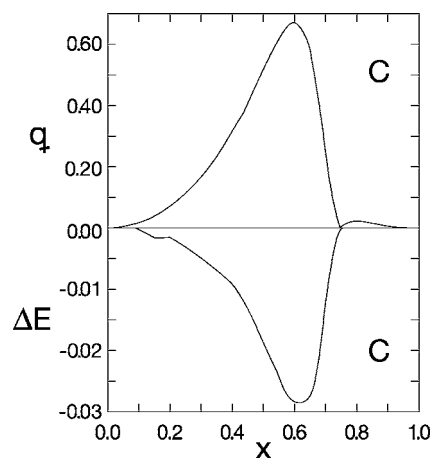


FIG. 3. Amplitude  $q$  of the Jahn-Teller distortion and energy gain  $\Delta E$  due to the Jahn-Teller coupling as a function of  $x$  for the  $C$  phase for  $E_{JT}=0.1t$  and  $\xi=0$  for all  $x$ .

elastic energy is almost completely compensated by the gain in energy due to the electron hopping. This scenario is favorable for a dynamical Jahn-Teller effect (in contrast to a static deformation).

### C. $C$ phase

In the  $C$  phase we consider antiferromagnetically oriented  $t_{2g}$  spins in the  $x$ - $y$  plane and these planes are then ferromagnetically correlated. As for the  $A$  phase the magnetic unit cell contains two Mn ions with opposite  $t_{2g}$  spin orientation. Both spin components of the  $e_g$  electrons have the same dispersion. As for the  $A$  phase the hopping is anisotropic and will drive a lattice distortion. The equilibrium value of  $q$  and the energy reduction  $\Delta E$  are presented in Fig. 3. As argued for the  $A$  phase  $q$  and  $\Delta E$  have to vanish in the limits  $x \rightarrow 0$  and  $x \rightarrow 1$ , and are maximum at intermediate  $x$ . The dependence of  $q$  and  $\Delta E$  on  $x$  is determined by the dispersion of the four bands and their occupation. Note the strong decrease of  $q$  around  $x=0.75$ . The small maximum of  $q$  for  $x \approx 0.8$  is associated with a very small energy gain.

Figure 4 shows the dependence of the energy ( $H_I + H_{JT}$ ) on  $\xi$  for  $x=0.35$  and  $x=0.60$ . The energy is minimal at

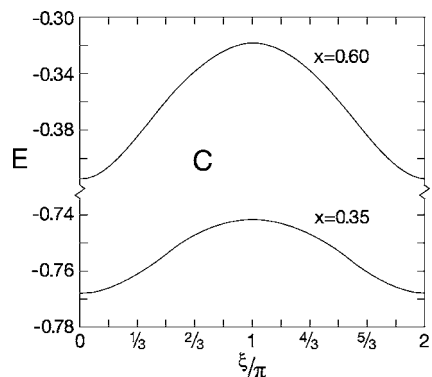


FIG. 4. Energy  $E$  corresponding to  $H_I + H_{JT}$  as a function of  $\xi$  for  $x=0.35$  and  $x=0.60$  in the  $C$  phase for  $E_{JT}=0.1t$ . The minimum of the energy is at  $\xi=0$ .

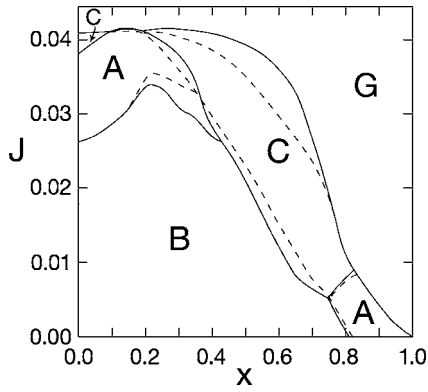


FIG. 5. Phase diagram obtained by comparing the ground state energies of the four phases as a function of  $J/t$  and  $x$  for the Mn ions on a cubic lattice. The dashed lines correspond to no Jahn-Teller coupling (Ref. 16) and the solid curves to  $E_{JT}=0.1t$ . The Jahn-Teller distortion only affects the A and C phases.

$\xi=0$  for all  $x$ .  $\xi=0$  corresponds to an expansion of the octahedron in the  $z$  direction while it contracts in the  $x$ - $y$  plane by keeping its volume constant. The strong decrease of  $q$  around  $x=0.75$  (see Fig. 3) is accompanied by a rather flat region of  $E(\xi)$  for  $|\xi| \leq \pi/2$ . Such flat dependence indicates that the system is susceptible to a dynamical Jahn-Teller distortion. As for the A phase, we have also allowed different  $\xi$  values for the two sublattices, but the energy minimum corresponds to equal  $\xi$  for all sites.

The above results explain the expansion of the  $c$  axis for the C phase. To study possible orbital order for this phase again larger unit cells with four Mn ions have to be considered, in analogy to the A phase. Staggered long-range orbital order is only stable if additional intersite correlations are taken into account.

#### D. G phase

In the G phase the spins are antiferromagnetically correlated, i.e., each up spin is surrounded by neighbors with down spins and vice versa. Hence, the electron hopping is always between sites of opposite spin and the  $a_{j\sigma}$  coefficients are all equal to  $1/\sqrt{2S+1}$ . The hopping is then the same along the three axis. As for the B phase, this isotropy does not favor a Jahn-Teller distortion. Indeed, the energy minimum is at  $q=0$  and hence the ground state energy is the same as in Ref. 16.

#### E. Phase diagram

The phase diagram is obtained by comparing the ground state energies of the four phases studied for a given  $x$ . The energy is determined in units of  $t$ , so that in the absence of Jahn-Teller effect there is only one dimensionless model parameter, namely,  $J/t$ . The corresponding phase diagram (calculated in Ref. 16) is shown in Fig. 5 with the set of dashed lines. The solid curves correspond to the phase diagram with a Jahn-Teller distortion for  $E_{JT}=0.1t$ .

Several energy crossovers are obtained for fixed  $x$  and as a function of the superexchange coupling  $J$ . For sufficiently

large  $J$  the G phase is always the groundstate; since all bonds are antiferromagnetic it has the lowest magnetic energy. The ferromagnetic B phase is favored at most values of  $x$  for small  $J$ . With increasing  $J$ , the ferromagnetism is rapidly quenched by the antiferromagnetic superexchange. The A and C phases are intermediate phases to the ferromagnetic B phase and the totally antiferromagnetic G phase. The Jahn-Teller distortion reduces the energy of the A and C phases and hence enhances the stability region for these two phases. Increasing  $E_{JT}$  of course further enhances the range of stability of the A and C phases. Since for  $x \approx 0$  and  $x \approx 1$  we have  $q \approx 0$ , there is no change of the phase diagram close to the compositional end points.

For  $x \approx 0$  the A phase should be stable over a wider range of  $J/t$  than shown in Fig. 5. So far the complicated nature of the  $\text{Mn}^{3+}\text{O}^{2-}$  bonds has been simplified by assuming cubic symmetry. Experimentally it is found that the length of ferromagnetic nearest neighbor bonds is considerably larger than the antiferromagnetic bonds. This is particularly evident in  $\text{LaMnO}_3$  (A phase), which is orthorhombic, but almost tetragonal,<sup>2</sup> with lattice parameters  $a \approx b \approx 0.399$  nm and  $c \approx 0.385$  nm. Hence, the  $c$  length is considerably smaller than  $a \approx b$ , i.e.,  $c/a < 1$ . On the other hand, the B and G phases are cubic corresponding to  $c/a=1$ , while for the C phase  $c/a > 1$ .<sup>2</sup> The actual lattice parameters strongly depend on the sample preparation.<sup>23</sup> In Ref. 16 we studied the phase diagram for anisotropic hopping and superexchange coupling to account for different lattice parameters. This approach slightly favors the A phase over the B phase, lowering the phase boundary to smaller values of  $J/t$ . The correct sequence for the phases as a function of  $x$ , namely, A-B-C-G, has been obtained in the range  $0.020 < J/t < 0.027$ . The Jahn-Teller effect in the limit  $x \rightarrow 0$  is briefly addressed in the next subsection.

The CE phase is the stable phase for a range of  $x$  between 0.5 and approximately 0.85. This phase has a complicated structure that in addition to an antiferromagnetic spin arrangement involves also charge order and antiferro-orbital order. The cell of the phase to be considered is quite large, which makes a calculation cumbersome. The slave-bosons project onto the  $\text{Mn}^{4+}$  configuration, i.e., they represent the charge, so that in order to study charge order the expectation value of the boson has to be different at different sites. The CE phase has not been included in Ref. 16 nor in the present paper.

Experimentally phase separation is often found at the boundary of the stability of phases.<sup>9</sup> Here regions of one phase are embedded in another phase giving rise to a coexistence of phases rather than a new mixed phase. For phase separation to occur the system has to gain energy through boundary conditions due to the finite size of the different regions. A system with separated phases is intrinsically inhomogeneous. For instance, inhomogeneities in the spatial distribution of Ca and La ions could locally induce phase separation. In our calculation we considered a homogeneous translationally invariant system and hence phase separation is excluded.

#### F. The $x \rightarrow 0$ limit

Since  $x=b^2$ , in the  $x \rightarrow 0$  limit the bandwidth due to hopping of the  $e_g$  electrons tends to zero as a consequence of the

correlations. This corresponds to a gradual localization of the  $e_g$  electrons due to a lack of holes to propagate. The system is an insulator due to the excluded multiple occupation of the sites. This is analogous to the physics of the  $t$ - $J$  model, where the kinetic energy is also renormalized as the band is filled. Hence, nominally all phases are metallic for  $x$  other than 0 and 1, and insulating for  $x=0$  and  $x=1$ . Note that for very small  $x$ , due to disorder scattering, the  $x$  holes are expected to be localized, so that the system is actually an insulator even if  $x \neq 0$ .

In this limit  $H_{JT}$  acts as a single-site crystal field and its contribution is purely static. From Eqs. (8) and (9) we see that under these circumstances it is energetically favorable to lift degeneracies. The eightfold degeneracy for the  $A$  phase (two sites per unit cell with two spin directions and two  $e_g$  orbitals each) can be lifted with a Jahn-Teller distortion and canting of the spins.<sup>24</sup> The latter induces a ferromagnetic component lifting the spin degeneracy. There is then a left-over twofold degeneracy per unit cell, which is able to accommodate the two  $e_g$  electrons per unit cell. Also if four Mn-sites per unit cell are considered with antiferro-orbital order, the degeneracy is lifted and only empty or full bands are obtained. Antiferro-orbital order must be driven by additional intersite interactions, which have not been included here. This scenario is roughly in agreement with the experimental findings.

Canting of the  $t_{2g}$  spins can be incorporated by introducing one canting angle in the hopping matrix element  $t$  within the  $xy$  plane and another canting angle for hopping along the  $z$  axis. The canting angles also affect the superexchange (magnetic energy) and the free energy has to be minimized with respect to the canting angles.

#### IV. CONCLUDING REMARKS

We considered a simple cubic lattice of intermediate valence Mn ions, with three localized  $3d$  electrons in the  $t_{2g}$  orbitals and correlated itinerant  $e_g$  electrons coupled to the lattice via the Jahn-Teller effect. The first of Hund's rules locally couples all the  $3d$  electrons ferromagnetically, maximizing the total spin at each site. The  $t_{2g}$  spins of the Mn ions interact with each other via a nearest neighbor superexchange, which competes with the double exchange caused by the hopping of the  $e_g$  electrons (formation of bonding and antibonding states between nearest neighbor sites). We considered the spin arrangements of the  $A$ ,  $B$ ,  $C$ , and  $G$  magnetic phases of  $\text{La}_{1-x}\text{Ca}_x\text{MnO}_3$ . The hopping of the  $e_g$  electrons depends on the orbital ( $x^2-y^2$  or  $z^2$ ) and on the magnetic phase. The excluded multiple occupation of the  $e_g$  levels at each site (due to large Coulomb interactions) is taken into account via slave bosons in the saddle point approximation. The Jahn-Teller modes  $Q_2$  and  $Q_3$  ( $\Gamma_3$  vibrational modes)<sup>20</sup> were taken into account as classical displacements (mean field).

The phase diagram is obtained by comparing the energies of the  $A$ ,  $B$ ,  $C$ , and  $G$  phases for each  $x$  and  $J/t$ . The hopping for the ferromagnetic  $B$  and antiferromagnetic  $G$  phases is isotropic and no Jahn-Teller distortions are obtained for these phases. The  $t_{2g}$  spin configuration in the  $A$  and  $C$  phases

gives rise to anisotropic hopping of the  $e_g$  electrons. It is unfavorable for an  $e_g$  electron with spin  $\sigma$  to hop to a site which has the  $t_{2g}$  spin pointing in the opposite direction. This is a consequence of the Clebsch-Gordan coefficients (Hund's rule), which strongly reduce the hopping amplitude. The Jahn-Teller distortion then reduces the ground state energy of the  $A$  and  $C$  phases and enhances the range of stability of these phases at the expense of the  $B$  and  $G$  phases. On the other hand, an external magnetic field stabilizes the ferromagnetic  $B$  phase. The Jahn-Teller distortions considered in this paper arise exclusively from the anisotropic hopping due to the spin configuration of  $t_{2g}$  spins. They explain the contraction of the  $c$  axis in the  $A$  phase and the expansion of the  $c$  axis in the  $C$  phase. It is also possible to induce different distortions of the octahedra by including noncubic crystalline field splittings and interactions between  $e_g$  electrons at neighboring sites. The latter is needed to induce staggered orbital long-range order.

Orbital order can as well be incorporated through local Coulomb and exchange interactions.<sup>25,26</sup> These interactions locally establish a preference for a given  $e_g$  orbital. The correlation between the sites is induced via Hund's rule coupling between the  $e_g$  and  $t_{2g}$  electrons and superexchange between  $t_{2g}$  spins. Depending on the implementation of the mean field, the phase diagram can be similar to the one presented here.<sup>26</sup>

The limit  $x \rightarrow 0$  is subtle because the correlations among the  $e_g$  electrons suppress the possibility of hopping and an insulator is obtained. In this limit the Jahn-Teller coupling is equivalent to a local crystalline field splitting and the system is prone to a canting of the spins<sup>24</sup> which reduces the ground state energy of the  $A$  phase. In Ref. 16 we considered changes in the hopping matrix element and the superexchange due to the different bond lengths for links with parallel or antiparallel  $t_{2g}$  spins. This again favors the  $A$  phase over the  $B$  phase as  $x \rightarrow 0$ . This way for  $J/t \approx 0.025$  we qualitatively reproduce the experimental sequence of phases as a function of  $x$ .

Some limitations of the present approach are as follows. (i) The complicated chemistry of the Mn-O bonds is only included through the intersite Mn-Mn hopping and the superexchange. (ii) The CE phase and the possibility of charge and orbital order are not considered. The CE phase has a larger unit cell and hence a more complicated band structure. Charge order, on the other hand, requires more than one expectation value for the slave bosons. (iii) Since we considered a translationally invariant lattice, a possible phase separation is suppressed.<sup>9</sup> A real space calculation, rather than a band approach in reciprocal space, is more adequate to discuss phase separation. (iv) It is assumed that the substitution of La by Ca does not introduce scattering of the  $e_g$  electrons.

The latter issue is related to the ionic radii of  $\text{La}^{3+}$  and  $\text{Ca}^{2+}$ ,  $r_{\text{La}^{3+}} = 1.03 \text{ \AA}$  and  $r_{\text{Ca}^{2+}} = 1.00 \text{ \AA}$ , respectively. These radii are very similar, so that no considerable volume change is expected solely as the consequence of the substitution. Moreover, the  $\text{O}^{2-}$  ions are going to be pulled slightly more toward a  $\text{La}^{3+}$  ion than toward  $\text{Ca}^{2+}$  because of the charge difference, reducing the effect further. The picture is very different for  $\text{La}_{1-x}\text{Sr}_x\text{MnO}_3$ , which nominally should behave similarly to the LCMO compound, but does not because the

ionic radius of  $\text{Sr}^{2+}$  is  $r_{\text{Sr}^{2+}}=1.18 \text{ \AA}$ , i.e., much larger than  $r_{\text{La}^{3+}}$ . For small  $x$  the phase diagram is still similar, but for large  $x$  the system is no longer single phase. The  $\text{Sr}^{2+}$  substitution intrinsically leads to larger mismatch. The situation can be improved by replacing La by Pr or Nd, which are also trivalent, but lead to smaller bandwidth (the hopping  $t$  through the O- $p$  orbital is reduced) so that the ferromagnetic phase is often not stable ( $J/t$  is larger now). The hopping  $t$  does not only depend on the cation radii, but also on the tolerance factor [ratio of the distance between the cation and O ions and the MnO bond length divided by  $\sqrt{2}$ , i.e.,

$d_{\text{C-O}}/(\sqrt{2}d_{\text{Mn-O}})$ ], which for perfect spheres would be one. In addition, these ions have  $4f$  electrons with their own magnetic properties interfering with the magnetism of the manganese ions.

#### ACKNOWLEDGMENTS

The support by the U.S. Department of Energy under Grant No. DE-FG02-98ER45707 and by the U.S. National Science Foundation under Grant No. DMR01-05431 is acknowledged.

- 
- <sup>1</sup>G. H. Jonker and J. H. van Santen, *Physica (Amsterdam)* **16**, 337 (1950); G. H. Jonker, *ibid.* **22**, 707 (1956).
- <sup>2</sup>E. O. Wollan and W. C. Koehler, *Phys. Rev.* **100**, 545 (1955).
- <sup>3</sup>R. von Helmolt, J. Wecker, B. Holzapfel, L. Schultz, and K. Samwer, *Phys. Rev. Lett.* **71**, 2331 (1993); K. Chahara, T. Ohuo, M. Kasai, and Y. Kozono, *Appl. Phys. Lett.* **63**, 1990 (1993); G. C. Xiong, Q. Li, H. L. Ju, S. N. Mao, L. Senapathi, X. X. Xi, R. L. Greene, and T. Venkatesan, *ibid.* **66**, 1427 (1995); Y. Tokura, A. Urishibara, Y. Moritomo, T. Arima, A. Asamitsu, G. Kido, and N. Furukawa, *J. Phys. Soc. Jpn.* **63**, 3931 (1994).
- <sup>4</sup>J. M. D. Coey, M. Viret, and S. Von Molnár, *Adv. Phys.* **48**, 167 (1999).
- <sup>5</sup>C. N. R. Rao and B. Raveau, *Colossal Magnetoresistance, Charge Ordering and Related Properties of Manganese Oxides* (World Scientific, Singapore, 1998).
- <sup>6</sup>*Physics of Manganites*, edited by T. A. Kaplan and S. D. Mahanti (Kluwer Academic/Plenum, New York, 1999).
- <sup>7</sup>E. Dagotto, T. Hotta, and A. Moreo, *Phys. Rep.* **344**, 1 (2001).
- <sup>8</sup>M. B. Salamon and M. Jaime, *Rev. Mod. Phys.* **73**, 583 (2001).
- <sup>9</sup>S. Yunoki, J. Hu, A. L. Malvezzi, A. Moreo, N. Furukawa, and E. Dagotto, *Phys. Rev. Lett.* **80**, 845 (1998); A. Moreo, S. Yunoki, and E. Dagotto, *Science* **283**, 2034 (1999); L. P. Gor'kov and V. Z. Kresin, *J. Supercond.* **12**, 243 (1999); P. Schlottmann, *Phys. Rev. B* **59**, 11484 (1999).
- <sup>10</sup>G. Zhao, K. Conder, H. Keller, and K. A. Müller, *Nature (London)* **381**, 676 (1996).
- <sup>11</sup>A. J. Millis, B. I. Shraiman, and R. Mueller, *Phys. Rev. Lett.* **77**, 175 (1996); Z. Popović and S. Satpathy, *ibid.* **88**, 197201 (2002); T. V. Ramakrishnan, H. R. Krishnamurthy, S. R. Hassan, and G. Venkateswara Pai, *ibid.* **92**, 157203 (2004).
- <sup>12</sup>G. J. Snyder, R. Hiskes, S. DiCarolis, M. R. Beasley, and T. H. Geballe, *Phys. Rev. B* **53**, 14434 (1996).
- <sup>13</sup>C. H. Booth, F. Bridges, G. J. Snyder, and T. H. Geballe, *Phys. Rev. B* **54**, R15606 (1996); S. J. L. Billinge, R. G. DiFrancesco, G. H. Kwei, J. J. Neumeier, and J. D. Thompson, *Phys. Rev. Lett.* **77**, 715 (1996).
- <sup>14</sup>B. B. Van Aken, O. D. Jurchescu, A. Meetsma, Y. Tomioka, Y. Tokura, and T. T. M. Palstra, *Phys. Rev. Lett.* **90**, 066403 (2003); M. C. Sánchez, G. Subías, J. García, and J. Blasco, *ibid.* **90**, 045503 (2003); X. Qiu, Th. Proffen, J. F. Mitchell, and S. J. L. Billinge, *ibid.* **94**, 177203 (2005).
- <sup>15</sup>J. Goodenough, *Phys. Rev.* **100**, 564 (1955).
- <sup>16</sup>P. Schlottmann, *Phys. Rev. B* **62**, 439 (2000).
- <sup>17</sup>C. Zener, *Phys. Rev.* **82**, 403 (1951); P. W. Anderson and H. Hasegawa, *ibid.* **100**, 675 (1955).
- <sup>18</sup>A. J. Millis, P. B. Littlewood, and B. I. Shraiman, *Phys. Rev. Lett.* **74**, 5144 (1995); N. Furukawa, *J. Phys. Soc. Jpn.* **64**, 2734 (1995); H. Röder, Jun Zang, and A. J. Bishop, *Phys. Rev. Lett.* **76**, 1356 (1996).
- <sup>19</sup>P. Schlottmann, *Phys. Rev. B* **60**, 7911 (1999).
- <sup>20</sup>J. Kanamori, *J. Appl. Phys.* **31**, 14S (1960).
- <sup>21</sup>S. E. Barnes, *J. Phys. F: Met. Phys.* **6**, 1375 (1976); P. Coleman, *Phys. Rev. B* **29**, 3035 (1984).
- <sup>22</sup>N. Read and D. M. Newns, *J. Phys. C* **16**, L1055 (1983).
- <sup>23</sup>Q. Huang, A. Santoro, J. W. Lynn, R. W. Erwin, J. A. Borchers, J. L. Peng, K. Ghosh, and R. L. Greene, *Phys. Rev. B* **58**, 2684 (1998).
- <sup>24</sup>P. G. de Gennes, *Phys. Rev.* **118**, 141 (1960).
- <sup>25</sup>R. Maezono, S. Ishihara, and N. Nagaosa, *Phys. Rev. B* **58**, 11583 (1998).
- <sup>26</sup>T. Maitra and A. Taraphder, *Phys. Rev. B* **68**, 174416 (2003).